Available online at www.sciencedirect.com

ScienceDirect

Procedia Structural Integrity 3 (2017) 484–497

Structural Integrity Procedia

www.elsevier.com/locate/procedia

XXIV Italian Group of Fracture Conference, 1-3 March 2017, Urbino, Italy

Creep behaviour of 15-15Ti(Si) austenitic steel in air and in liquid lead at 550°C

A. Strafella*, A. Coglitore, E. Salernitano

ENEA- Italian National Agency for New Technologies, Energy and Sustainable Economic Development-Laboratory of Materials Technologies Faenza, Via Ravegnana, 186 - 48018 - Faenza, Italy

Abstract

This work aims at studying the creep behaviour of 15-15Ti(Si) austenitic steel, under uniaxial stress and its interaction with liquid lead. Creep tests were performed at 550 °C in an engineering stress range of 300-560 MPa. The 15-15Ti(Si) stainless steel is one of the best candidates for the nuclear reactor components of IV generation Lead-cooled fast reactor (LFR) and was tested in air and in stagnant liquid lead to simulate its behaviour in operating thermal and mechanical stress conditions and to verify its sensitivity to Liquid Metal Embrittlement (LME). Only few data can be found in the literature on 15-15Ti(Si) characterization, therefore the performed tests provided important information to use this material in the nuclear field, allowing to obtain the characteristic curve simulating the creep behaviour in air at all stress values, based on the Norton law and experimental data. The results of the specimens in air were compared with those obtained in lead, providing important information on creep corrosion: the liquid metal embrittlement effect takes place in lead and it produces a decrease of creep-rupture time, a reduction of creep strain and then the loss of steel ductility. Moreover, Scanning Electron Microscope (SEM) micrographs highlighted that lead changes both the mode and the type of specimen fracture. In addition, it was analyzed the lead action time, as the time after which the corrosion appears with macroscopic effects. These tests are still in progress: up to the current value of time (800h), they showed similar creep behaviour of the specimens tested in air and in lead. It can be assumed that liquid metal embrittlement takes place after a long time of steel/lead contact. However, since these tests are ongoing, these results will be object of our future studies.

Copyright © 2017 The Authors. Published by Elsevier B.V. This is an open access article under the CC BY-NC-ND license (http://creativecommons.org/licenses/by-nc-nd/4.0/).
Peer-review under responsibility of the Scientific Committee of IGF Ex-Co.

Keywords: 15-15Ti(Si); austenitic stainless steel creep; creep curves; steady strain creep rate; Liquid Metal Embrittlement (LME); creep tests in lead

* Corresponding author.
E-mail address: alessandra.strafella@enea.it

Copyright © 2017 The Authors. Published by Elsevier B.V. This is an open access article under the CC BY-NC-ND license (http://creativecommons.org/licenses/by-nc-nd/4.0/).
Peer-review under responsibility of the Scientific Committee of IGF Ex-Co.
10.1016/j.prostr.2017.04.061

1. Introduction

In the nuclear field, austenitic stainless steels are the best candidates for high temperature components of fast reactors. Creep strength and resistance to irradiation-induced void swelling are the main requirements of the austenitic stainless steels. Type 15-15Ti(Si) material is a Ti-stabilized austenitic stainless-steel alloy of particular interest to the nuclear industry (Latha et al. (2008), Gilbon et al. (1987), IAEA Report).

15-15Ti(Si) with specifically tailored composition, especially regarding the carbon and titanium content, have been designed around the standard AISI 316 stainless steel such that the modified grade exhibited lower irradiation induced void swelling (Latha et al. (2008)). The addition of Ti improves the high temperature mechanical properties due to the precipitation of carbide particles, either $M_{23}C_6$, or TiC in relation to the contents of Ni and Cr and to the matrix structure, grain size and dislocation density. Ti-modified austenitic stainless steels are often cold-worked to increase their mechanical properties. Therefore, the cold-worked steels have higher crack growth resistance at high stress intensity levels compared to solution-annealed stainless steel. The cold-working promotes the precipitation of carbides which are liable to precipitate on slip planes produced by pre-strain and creep strain (Caro et al., Vaidya (1983), Wilson et al (1968), Daenner (1981)).

Austenitic stainless steels will have to be used for nuclear reactor components of IV generation Lead-cooled fast reactor (LFR). A liquid lead cooled nuclear reactor is one of the systems to be deployed in the future; the main problem in LFR reactor development is the compatibility of the structural materials (steels) with the coolant as well as the corrosion of structural components and fuel. When steel comes in contact with liquid metal, the Liquid Metal Embrittlement (LME) could occur, that is the loss of ductility in normally ductile metals when stressed under contact with liquid metal.

15-15Ti(Si) is one of the best candidates for high temperature components of LFR (Gilbon et al (1987), IAEA Report). Although there is a great interest on these steel properties, only few data on its characterization can be found in the literature.

So, the aim of this work is a preliminary study of the 15-15Ti(Si) stainless steels creep properties at 550° C both in air and in lead.

Nomenclature

BSE	Backscattered electrons
CW	Cold worked
LFR	Lead-cooled fast reactor
LME	Liquid Metal Embrittlement
$R_{p0.002}$	Yield stress
SE	Secondary electrons
SEM	Scanning Electron Microscope
SLVC	Super Linear Variable Capacitor transducer
sscr	Steady strain creep rate

2. Experimental procedure

2.1. Materials

Tests were carried out on creep specimens prepared from 15-15Ti(Si) steel, an austenitic steel provided by OCAS. The steel was manufactured in the form of plates (15mm X 750mm X 250mm), 20% cold-worked (CW): it was subjected to a homogenization annealing treatment in a furnace at 1230°C for 15h, hot-rolled at 1250°C for 1.5-2h, annealed at 1080°C (followed by a water-quench treatment) and 20% CW.

The cold-working promotes the precipitation of carbides, which generally increases the mechanical properties of materials. The composition of 15-15Ti(Si) is given in Table 1.

Table 1. Chemical composition of 15-15Ti(Si) steel (wt %).

C	Mn	Si	P	Ti	Cr	Ni	B	Mo
0.090	1.502	0.791	0.041	0.404	14.392	15.607	0.007	1.509

Ti addition improves the high temperature mechanical properties due to the precipitation of carbide particles, either $M_{23}C_6$, or TiC in relation to the contents of Ni and Cr and to the matrix structure, grain size and dislocation density. Compared to solution-annealed stainless steel, the cold-worked steels have higher crack growth resistance at high stress intensity levels. Moreover, the Ti presence decreases the irradiation swelling in steel used for nuclear applications.

The used lead is provided by Sigma-Aldrich in particles with a purity ≥ 99.9%, size ≤ 2 mm and melting point 327.4°C.

2.2. Specimens

Creep specimens were machined from the plate in the rolling direction to obtain 6 mm in diameter and 70 mm of gauge length, as shown in Figure 1.

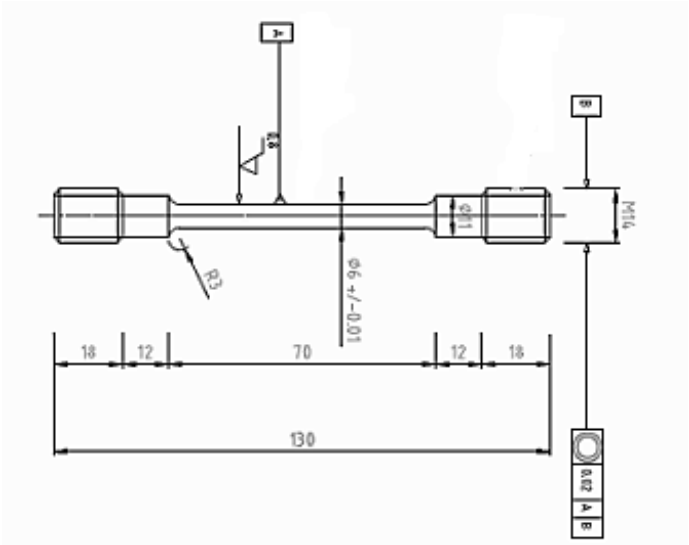

Fig. 1. Creep specimen dimensions.

2.3. Creep tests

The creep tests were carried out in air and in stagnant lead, at 550°C that is typical working temperature of LFR. The loads were applied in uniaxial tensile mode; stress values were in the range of 300-560 MPa, which is lower than yield stress value (theoretical 620 MPa ≤ $R_{p0.002}$ ≤ 840 MPa, after 20% CW).

All tests were performed by MAYES machine with a maximum loading capacity of 20kN and maximum temperature of 1000°C. Because of the measurement uncertainty in the determination of the specimen cross section, the initial tensile stress was measured with an accuracy of ±3%. The specimen elongation during the tests was measured by monitoring in continuous the grip movement; Super Linear Variable Capacitor (SLVC) transducers were used for measuring and recording elongations smaller than 0.5 μm. The acquired data were plotted as conventional strain versus time curves. The matrix of main tests is shown in Table 2.

Table 2. Matrix of the main tests.

Material	Temp. [°C]	Stress [MPa]			
		300	400	560	575
15-15Ti(Si)	550°C	○	○	○, ●	●

where "○" represents the creep test performed in air and "●" that in lead. A particular cell, showed in Figure 2, was specifically designed and manufactured for tests in lead.

Fig. 2. Cell designed and manufactured for tests in lead, mounted on a MAYES machine.

The cell is mounted on a MAYES machine; specimen was fixed to the grips of cell, filled with solid lead, heated up to the lead melting temperature and then the test temperature and load were applied. Data points were acquired every 1 h.

After rupture, the specimens were cut under fracture surface to be analyzed with a SEM Leo 438 VP to characterize the morphology and microstructure of the fracture surfaces.

The observations were performed in high vacuum, with no need of surface preparation treatments. Both the secondary (SE) and backscattered electron (BSE) detectors were used to point out morphological and chemical features.

SE are emitted from the sample top surface atoms providing information relating exclusively to the surface morphology, while BSE are issued from the deeper layers of the material (up to about one micron deep) providing information relating to the composition and to the topography of the sample.

3. Results and discussion

3.1 Creep curves in air

The specimens were tested at 550°C under constant loads, corresponding to the initial tensile stresses in the range of 300-560 MPa, and the experimental data allowed to obtain the typical creep curves of 15-15Ti(Si). The most relevant curves were depicted in Figure 3, where the evolution of the creep strain with time at various stress levels is plotted.

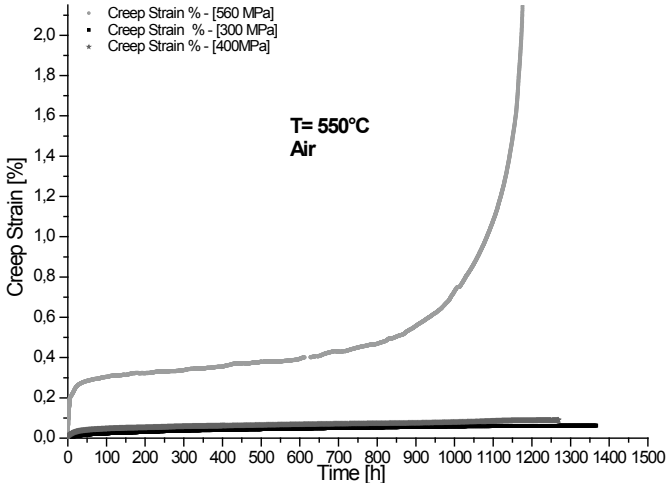

Fig. 3. Comparison of 15-15Ti(Si) creep curves in air at 300, 400, 560 MPa.

The creep strain at the same time value increased with the applied stress and the shape of creep curve is consistent with the expectations: at 300 and 400 MPa, after 1200 h, the strain curves didn't reach the tertiary creep stage, still remaining in the secondary creep phase. At stress values near the yield strength of 15-15Ti, as 560MPa (theoretical 620MPa $\leq R_{p0.002} \leq$ 840MPa, after 20%CW), all the three phases of creep can be recognized.

During the test at 560MPa, the rupture was reached at 1165h, unlike the tests at 300 and 400MPa still in progress, whose curves are plotted in Figure 4. These tests provide important results on the creep behaviour because the secondary creep stage was reached and the duration was greater than of 1200h.

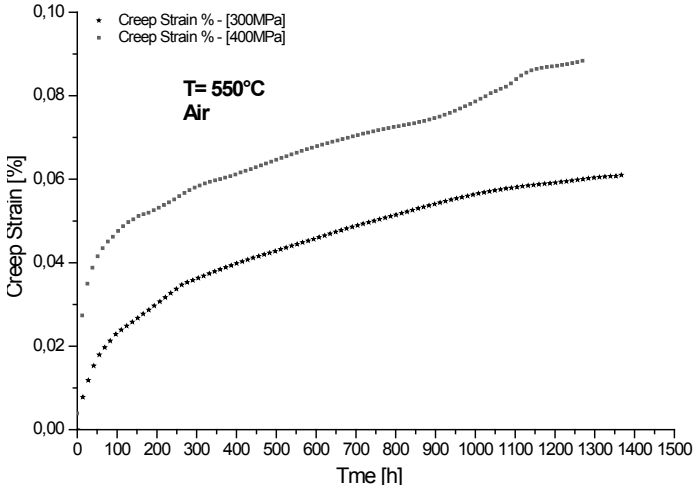

Fig. 4. Comparison between creep curves in air at 300 and 400 MPa.

All tests enabled to calculate the creep rate of secondary stage, also defined steady strain creep rate (sscr) being the minimum and constant creep rate.

The sscr values are obtained and compared with two methods, as illustrated in Figure 5:

- Plotting Fit linear of strain-time curve in secondary creep stage
- Using the first derivative on curve strain-time to determinate the minimum

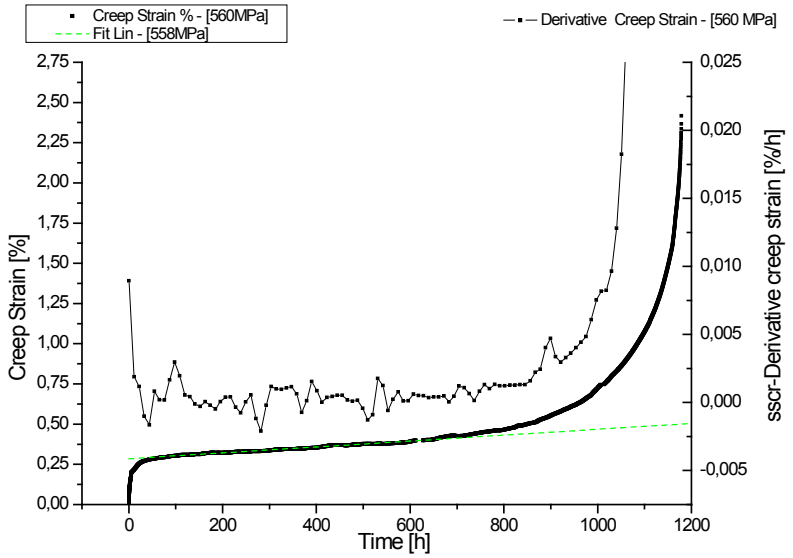

Fig. 5. Typical sscr calculus: minimum of first derivative and fit linear of secondary creep stage.

The steady strain creep rates were plotted in a log–log graph. Figure 6 shows the variation of sscr with the applied stress.

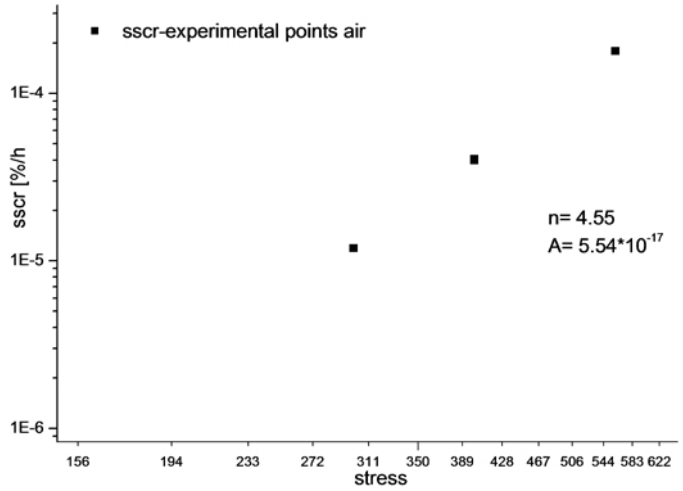

Fig. 6. log–log plot of sscr-stress points.

The variation of sscr with applied stress obeys a power law relationship in the form of Norton-type:

$$sscr = A\sigma^n \tag{1}$$

where **σ** is the applied stress, **n** is the stress exponent, and **A** is an empirical constant.

For 15-15Ti(Si) steel, the found **A** and **n** values are showed in Table 3.

Table 3. Values of Norton-power law parameters

A	n
$5.54*10^{-17}$	4.5

The value of stress exponent **n** is indicative of the rate controlling deformation mechanism.

The 15-15Ti(Si) austenitic steel showed a value for the stress exponent n =4.5. This result is consistent with the expectations, since in austenitic stainless steels stress exponents are generally in the range of 3–12 and are associated with dislocation creep [Caro et al.]. This is due to the nature of austenitic stainless steels which are solid solution alloys where the precipitation takes place during creep; for this reason, they show a particular behaviour which is intermediate between those of solid solution alloys and precipitation hardened/dispersion strengthened materials.

The literature data report a value of n=3–5 for pure metals and simple solid solution alloys where the main creep deformation mechanism is the dislocation creep; other major creep deformation mechanisms such as diffusion creep are characterized by n= 1, and grain boundary sliding controlled creep are identified with a value of n =2.

Instead, as also reported by literature, complex alloys and precipitation hardened/dispersion strengthened materials showed much higher values of n (≈40). It means that in austenitic stainless steels, the value of **n** is intermediate between those of solid solution alloys and precipitation hardened/dispersion strengthened materials and it is in a range of 3–12 [Caro et al.].

The value of stress exponent n= 4.5 obtained in these tests confirms that 15-15Ti(Si) deforms through the dislocation creep mechanism.

Based on the Norton power law, on experimental data and on calculated values of **n** and **A**, the characteristic creep curve sscr-stress (log–log plot) was plotted, enabling to simulate the creep behaviour in air at all stress values (Fig.7).

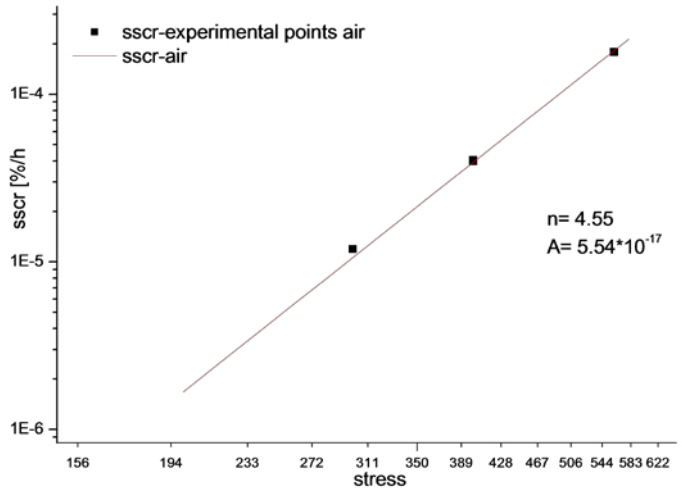

Fig. 7. Characteristic creep curve sscr-stress.

Since only few data can be found in the literature on 15-15Ti(Si) characterization, these analyses could provide some important information for the use of this material in nuclear field.

3.2 Creep curves in lead

For its particular application on nuclear field, 15-15Ti(Si) was tested in lead in order to conduct a preliminary study on its lead corrosion sensitivity. Generally, the same conditions chosen for the test in air were used. One of the most important tests in lead was performed using the following parameters, that are the conditions for which the creep test in air reached the rupture:

- T= 550°C
- σ = 560MPa

To date, this test is still in progress: the strain is 0.5% and the test duration is 800h, as depicted in Figure 8.

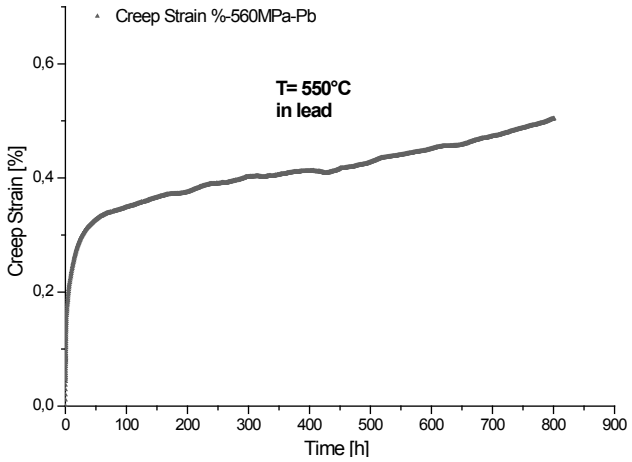

Fig. 8. Creep curve of specimen tested at 560MPa in lead.

It can be observed that, as well as the test in air, at this stress value primary and secondary phases of creep can be recognized and the calculation of sscr was possible.

Creep curve obtained from the test on specimen in air was compared with that obtained in lead. The comparison between creep curve in air and in lead at 560MPa is depicted in Figure 9.

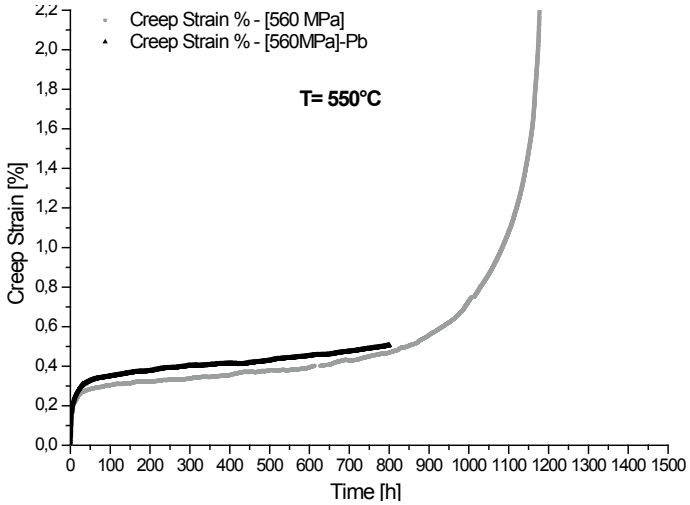

Fig. 9. Comparison of 15-15Ti(Si) creep curves in air and in lead.

As expected, an increase in creep strain was observed, but it isn't really relevant since until the current value of test in lead (800h), it can be observed that:

- the shape of creep curve in lead and in air is the same
- the difference of creep strain percentage between the curve in air and the curve in lead is around 0.04% and it concerned only the primary creep
- the strain rate is the same

The value of sscr obtained by the test in lead was plotted in the same graph of log-log sscr-stress curve in air (Figure 10).

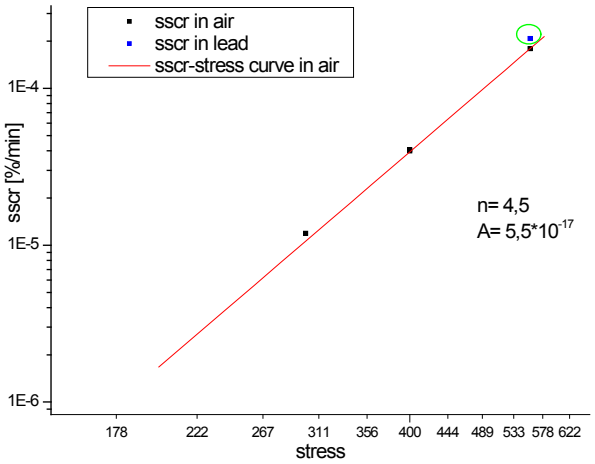

Fig. 10. sscr value plotted on sscr-stress curve in air graph.

Up to the current value of time (800h), the behaviour of 15-15Ti(Si) in lead and in air at 560 MPa is almost similar. For the test in lead, creep mechanisms seem to be predominant than lead corrosion, although it occurs with an increase of deformation. It could be ascribable to the stress value near yield stress[1] and it can be hypothesized that lead corrosion appears after a long time of steel/lead contact. These considerations will be the focus of our future studies.

To understand the effect of lead corrosion, it is necessary to discuss a further test in lead at higher stress level. This preliminary test was performed at 575MPa to ascertain the correct working of new cell designed and manufactured for tests in liquid metal.

Test conditions were the following:

- T= 550°C
- σ= 575MPa
- In lead

As shown in Figure 11, creep behaviour in lead at 560MPa and at 575MPa is similar; unlike test at 560MPa which is in progress, test at 575MPa finished and the specimen broke.

[1] theoretical 620 MPa ≤ $R_{p0.002}$ ≤ 840 MPa, after 20% CW

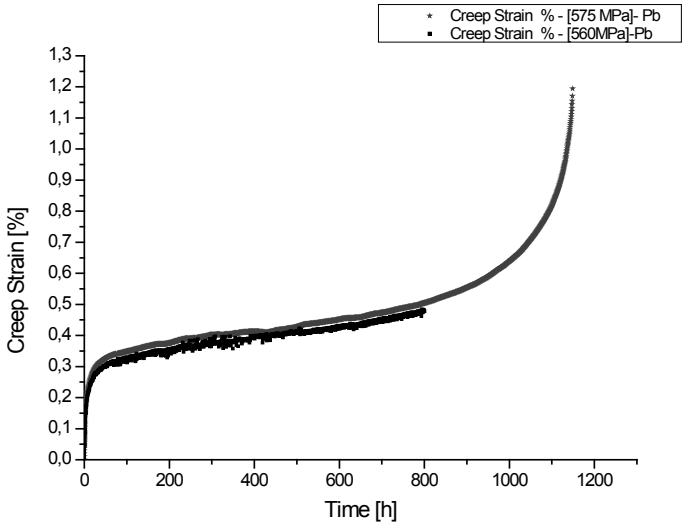

Fig. 11. Comparison between creep curves in lead at 560MPa and 575MPa.

Although they weren't obtained at the same stress level, creep curve at 560MPa in air and at 575MPa in lead are plotted in Figure 12 because this comparison can provide important information on creep corrosion, even more that the stress difference falls within the tolerance limit of accuracy (±3%, as stated in paragraph 2.3). Rupture time of specimen tested at 575MPa in lead is lower than that tested in air at 560MPa, as expected.

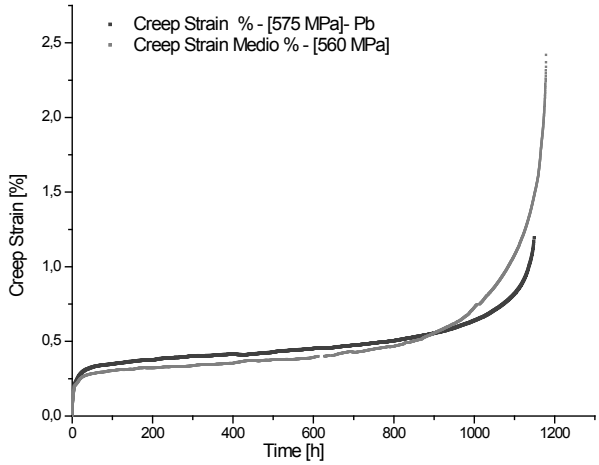

Fig. 12. Comparison between creep curves at 560MPa in air and at 575MPa in lead.

Up to 850h, creep strain of sample in lead is higher than creep strain in air and this supports the hypothesis that lead corrosion appears after a long time of steel/lead contact. For time greater than 850h, it can be observed a trend inversion. Although subjected to higher stress level, the specimen tested at 575MPa in lead shows a lower percentage of final creep strain than specimen tested at 560MPa in air, but it shows a lower time of rupture too; this means that it is less ductile than specimen tested in air and it is in accordance with LME effect.

It is important to underline that these tests in stagnant liquid lead were performed to verify the steel sensitivity to LME. The *Handbook on Lead-bismuth Eutectic Alloy and Lead Properties, Materials Compatibility, Thermalhydraulics and Technologies* [NEA Expert Group (2015)] proposes the following definition of LME*: LME is the loss of ductility of a normally ductile metal or metallic alloy when stressed in contact with a liquid metal that can result in*

brittle fracture. Typically the phenomenon is accompanied with a change from ductile to brittle fracture modes, intergranular or transgranular cleavage-like fracture modes.

According to this definition, the LME justifies the decrease of rupture time, the reduction of creep strain and then the loss of specimen ductility tested in lead.

3.3 Microstructure of fracture surfaces

The specimens were examined after rupture by scanning electron microscopy. Secondary electrons are used to obtain the fracture surface morphology.

Typical SEM images of fracture surfaces obtained from the creep specimens are shown in Figure 13.

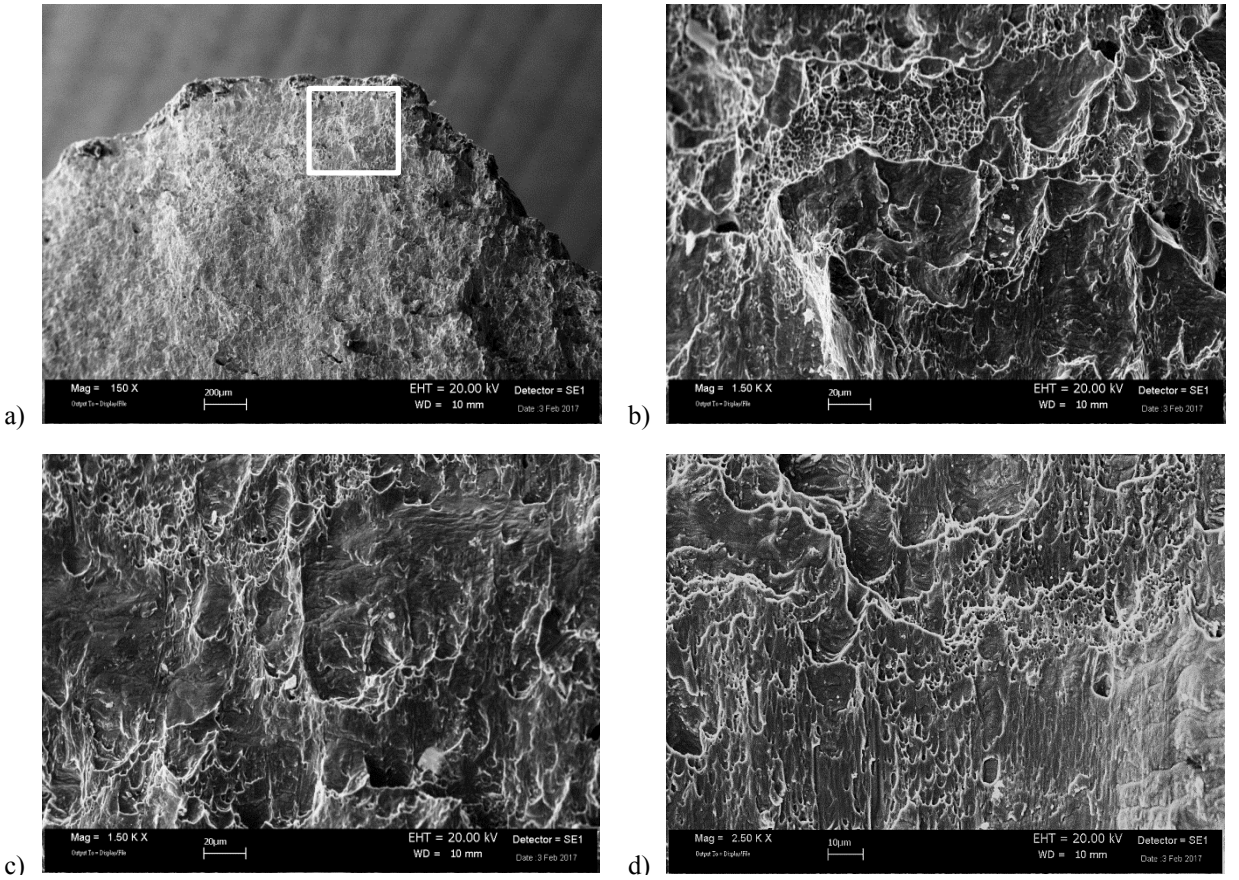

Fig. 13- SEM micrographs: a) fracture surface at low magnification; b) portion of surface showing a mixed ductile/brittle fracture mode; c) portion of surface showing a dominant transgranular fraction and a little presence of ductile fraction; d) deformation bands.

Micrographs of some regions of a fracture surface show a combination of cup-cone and transgranular fracture modes. A transgranular fracture mode seems to be dominant in other regions; for example, it is the characteristic feature for central part of specimen where fracture along cleavage planes is noticed (Fig 13.c). The other portions of the fracture surface are a combination of shear rupture (transgranular rupture) and cup-cone fracture (coalescence by shear of voids caused by plastic deformation). In these areas, the transgranular rupture is incomplete and they are characterized by a mixed rupture mode, as in the case of external surface corresponding to necking of specimen or in the case of surface close to central area of specimen (Fig 13. b) and d)). These observations are consistent with the expectations: the addition of Ti improves the high temperature mechanical properties, as creep strength, due to the precipitation of carbide particles, as reported by Zahra and Schroeder (1982). They studied creep properties of an

austenitic steel with a chemical compositions similar to that of 15-15Ti(Si), finding that the fine TiC precipitates in Ti-stabilized austenitic stainless-steel cold-worked alloy form preferentially on the intergranular dislocations and they are more stable [Zahra and Schroeder (1982)]. This justifies transgranular fracture.

Finally, it can be concluded that the specimen rupture mode is mixed, transgranular and cup-cone, with greater percentage of transgranular rupture area.

Even for specimen tested in lead, chemical and morphological features of fracture surface was analyzed by Scanning Electron Microscopy (Figure 14).

Using backscattered electrons detector, it is possible to differentiate steel surface fracture and eventual lead residues, being the micrograph contrast determined by the atomic number of the elements in the sample.

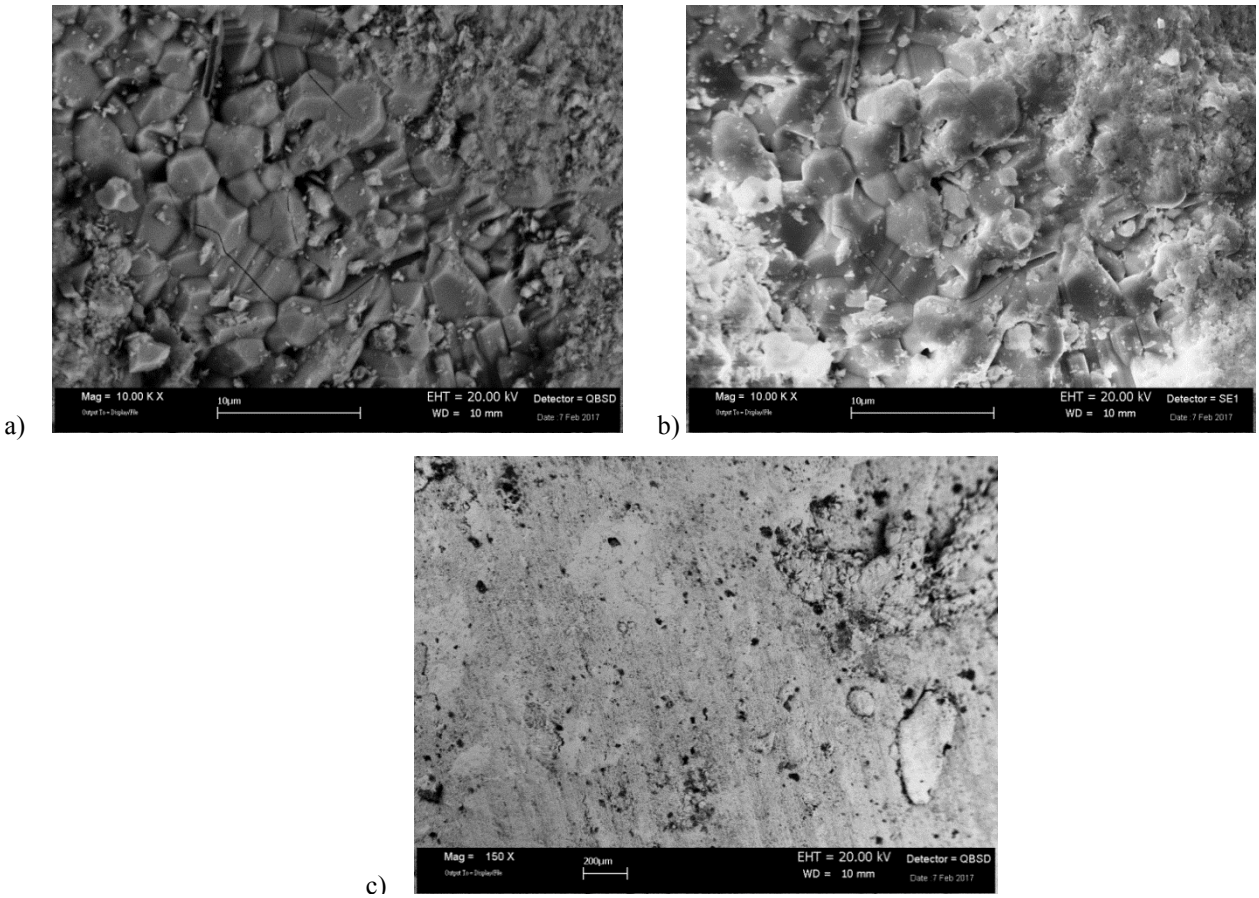

Fig. 14. SEM micrographs: surface portion showing typical intergranular fracture observed both with a) BSE detector and b) SE detector; c) fracture surface at low magnification showing a fully brittle fracture.

It can be concluded that the fracture is brittle, as showing by the typical intergranular fracture of Figure 14, where the decohesion occurring along a weakened grain boundary is evident. Grains are clearly observed in their three-dimensional structure (Figure 14 a) and b)). Figure 14- c) depicts a polished fracture surface with no wrinkled appearance, unlike ductile materials.

It can be noticed that the fracture mode is different from that of specimen broken in air: a mixed fracture mode, cup-cone/transgranular, characterizes the specimen tested in air while intergranular fracture mode characterizes the specimen tested in lead.

The loss of steel ductility is also evident from images in Figure 15 showing the specimen immediately after rupture: there are macroscopic differences between the two fracture surfaces.

a) 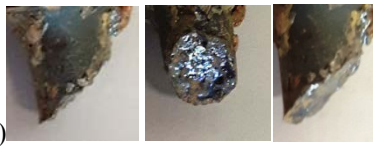 b) 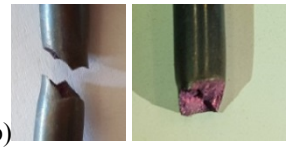

Fig. 15. Fracture surfaces immediately after rupture: a) specimen tested at 575MPa in lead; b) specimen tested at 560MPa in air.

The Figure 15-a) shows the typical brittle fracture, along 45°, with negligible plastic deformation. The fracture surface is brilliant and polished. Figure 15-b) highlights both the specimen necking, which identifies the ductile fracture, and the typical changes of fracture direction, which characterizes the transgranular fracture. The fracture surface has a wrinkled appearance of mixed or ductile fracture.

The difference of these fracture modes is ascribable to the effect of lead embrittlement: the transition from mixed fracture mode, ductile-brittle/transgranular, which takes place in air to fully brittle/intergranular mode, in lead, is consistent with the definition of LME (stated in paragraph 3.2) and with the creep phenomena in liquid metal, as described in other scientific works.

According to Hough and Rolls (1971), phenomena associated with creep rupture in liquid metal can include:

- cracking induced by the adsorption of liquid metal atoms
- accelerated failure due to the penetration of the liquid metal along the grain boundary of the solid
- stress - aided dissolution of metal from a crack tip

These conclusions can justify the intergranular fracture mode: intergranular fracture usually occurs when the phase in the grain boundary is weak and brittle and this is probably due to the penetration of the liquid metal along the grain boundary of the steel which caused the embrittlement of phases and then the accelerated failure.

It means that lead changes both mode and type of fracture: from mixed ductile/brittle to total brittle and, referring to brittle mode, from transgranular to intergranular type. That is the effect of liquid metal embrittlement.

Conclusions

Creep behaviour of 15-15Ti(Si) austenitic stainless steel has been investigated at 550°C in a stress range of 300-575MPa. Tests were performed in air and in lead.

For what concerns specimens tested in air, it was obtained typical creep curve strain-time, it was calculated **n** and **A**, parameters of the Norton power law, and it was found that 15-15Ti(Si) deforms through the dislocation creep mechanism. Based on the Norton power law, on experimental data and on calculated values of **n** and **A**, it was plotted the characteristic creep curve sscr-stress (log–log plot) which can enable to simulate creep behaviour in air, at all stress values.

SEM micrographs show that the specimen fracture mode in air is mixed, transgranular and cup-cone, with greater percentage of transgranular rupture area.

Tests in lead were also performed, some of which are still in progress, as test at 560MPa. Up to now (duration 800h), the comparison between creep curves of specimens tested at 560MPa in air and in lead point out a very similar behaviour. Creep mechanisms seem to be predominant than the lead corrosion, although it occurs with an increase of deformation. It could mean that the lead corrosion occurs after a long time of steel/lead contact. However, the test at 560MPa is still ongoing and these results will be the subject of our future studies.

Another important test in lead was a preliminary test at 576MPa which was performed as first test to ascertain the correct working of new cell designed and manufactured for tests in liquid metal. At current value of time (800h), the creep behaviour in lead at 560MPa and at 575MPa is similar. Moreover, unlike test at 560MPa, that at 575MPa finished and the specimen broke. For these reasons, creep curve in lead at 576MPa was compared with creep curve in air at 560MPa.

This comparison can help to better understand the creep corrosion mechanisms: there is the liquid metal embrittlement effect which justifies the decrease of rupture time, the reduction of creep strain and then the loss of steel ductility tested in lead.

The same conclusions were provided by SEM micrographs on specimen tested in lead: it can be observed that typical intergranular fracture took place. Moreover, the differences between mixed fracture mode, ductile-brittle/transgranular, occurring in air and fully brittle/intergranular mode, in lead were showed. It means that lead changes both the mode and the type of fracture from mixed ductile/brittle to total brittle and, referring to brittle mode, from transgranular to intergranular type, as a consequence of liquid metal embrittlement.

Since only few data on 15-15Ti(Si) characterization can be found in the literature, these analyses could provide some important information for the use of this material in nuclear field.

Acknowledgement

The authors are grateful to Dr. Selene Grilli for her careful revision of the manuscript. We also acknowledge the C.R. ENEA Brasimone for financial support and providing the samples to be tested.

References

Abou Zahra, D-A., Schroeder, H., 1982. The dependence of the creep properties of DIN 1.4970 austenitic stainless steel at 973 K on different thermomechanical pre-treatments. Journal of Nuclear Materials 107, 97-103, North.Holland Publishing Company.

Caro, M., Woloshun, K., Rubio, F., Maloy, S., Materials Selection for the Lead-Bismuth Corrosion and Erosion Tests in DELTA Loop Los Alamos National Laboratory.

Daenner, W., 1981. A comparison of AISI type 316 and German type DIN 1.4970 stainless steel with regard to the first-wall lifetime. Journal of Nuclear Material 103 & 104, 121-126. North.Holland Publishing Company.

Gilbon, D., Séran, T.L., Maillard, A., Touron Rivera, H.C., Lorant, H., Permet, J., Rabouille, O., 1987. Swelling microstructure of neutron irradiated Ti-stabilized austenitic steels. International conference on materials for nuclear reactor core applications, Bristol (UK) 27-29 Oct 1987.

Hough, R.R., Rolls, R., 1971. Creep fracture phenomena in iron embrittled by liquid copper. Journal of Material Science 6, 1493-1498.

IAEA, International Atomic Energy Agency. Nuclear Energy Series Technical Reports Structural Materials for Liquid Metal Cooled Fast Reactor Fuel Assemblies — Operational Behaviour No. NF.T.4.3 Guides.

Latha, S., Mathewa, M.D., Parameswaran, P., Bhanu Sankara Rao, K., Mannan, S.L., 2008. Thermal creep properties of alloy D9 stainless steel and 316 stainless steel fuel clad tubes. International Journal of Pressure Vessels and Piping 85, 866–870.

NEA Expert Group on Heavy Liquid Metal Technologies, 2015. Handbook on Lead-bismuth Eutectic Alloy and Lead Properties, Materials Compatibility, Thermalhydraulics and Technologies- Nuclear Energy Agency Organisation For Economic Co-Operation And Development, 487-570.

W.V. Vaidya Gkss, 1983. Radiation-induced recrystallization, its cause and consequences in heavy-ion irradiated 20% cold-drawn steels of Type 1.4970. Journal of Nuclear Materials 113, 149-162 North.Holland Publishing Company.

Wilson, F. G, Pickering, F. B., 1968. A study of zone formation in an austenitic steel containing 4% Titanium. Acta Metallurgica, 16, 115-131.